Journal of MATERIALS RESEARCH

Article
DOI:10.1557/s43578-024-01348-y

Influence of electrochemical hydrogen charging on the mechanical, diffusional, and interfacial properties of an amorphous alumina coating on Fe-8 wt% Cr alloy

Hariprasad Gopalan[1,a)], Jing Rao[1], Piyush Patil[1], Chanwon Jung[1], Se-Ho Kim[1,2], Silas Goodrich[1], Marcel Wetegrove[3], Angela Kruth[3], Christina Scheu[1,a)], Gerhard Dehm[1,a)], Maria Jazmin Duarte[1]

[1] *Max-Planck-Institut Für Eisenforschung GmbH, Düsseldorf, Germany*
[2] *Department of Materials Science and Engineering, Korea University, Seoul 02841, Republic of Korea*
[3] *Leibniz Institute for Plasma Science and Technology (INP), Greifswald, Germany*
[a)] Address all correspondence to these authors. e-mails: hariprasad.gopalan@iitrpr.ac.in; scheu@mpie.de; dehm@mpie.de

Received: 7 November 2023; accepted: 17 April 2024; published online: 6 May 2024

Amorphous alumina coatings, intended as hydrogen barriers, were successfully deposited on Fe-8 wt% Cr substrates by plasma ion-assisted deposition technique. The amorphous structure of the coatings was confirmed by transmission electron microscopy and X-ray diffraction. The interfacial and mechanical properties of the coating-substrate system were evaluated using an in-house custom-designed backside electrochemical hydrogen charging method. In this approach, the substrate side faces the electrolyte (hydrogen entry side) and the mechanical behavior was tested on the coating side (hydrogen exit side). A Kelvin-probe-based measurement was performed to determine the hydrogen diffusivity in these amorphous alumina coatings at room temperature using a similar backside charging approach. Chemical and microstructural characterizations, in combination with scratch and hardness testing, show that interfacial hydrogen accumulation is strongly responsible for drastic changes in the scratch morphology of the coating and its adhesion to the substrate. Scratch testing promises to be a quick and easy technique to fingerprint changes at the coating/substrate interface upon hydrogen exposure.

Introduction

Alumina (aluminum oxide) coatings are an excellent choice for hydrogen barrier applications [1]. Particularly, crystalline alumina is known for high-temperature permeation resistance towards hydrogen and its isotopes for nuclear applications [2]. The permeation rate at 1000 K in a 1-μm-thick film alumina-coated substrate system is 3–4 orders of magnitude lower compared to the bare steel substrate [3]. On the other hand, ambient temperature transport of hydrogen gas through pipelines will become important in a much anticipated switch towards a hydrogen fuel-driven economy [4]. Structural high-strength ferritic steels are vulnerable to hydrogen-induced embrittlement at these temperatures [5]. Therefore, there is a need to develop coatings with good hydrogen barrier resistance, mechanical properties, and excellent coating–substrate adhesion. For instance, amorphous alumina in thin film form has shown significantly improved tensile ductility [6], making it less vulnerable to early failure by cracking. Furthermore, hydrogen permeation of amorphous alumina-coated steels at 323–333 K is reported to be reduced by 3–4 orders of magnitude compared to the glass substrate [7]. In a recent review, we summarize the different methodologies to measure hydrogen diffusivity, which also explains the large scatter of the available data [8]. Hydrogen permeation mechanisms in coating-substrate systems can be controlled by surface dissociation, diffusion, and/or solubility limited regimes in the coatings [1]. The sequential nature of these processes makes the slowest mechanism as rate controlling, which is challenging to delineate at room temperature as all the involved mechanisms are thermally activated (therefore, very slow at room temperature). As a first step we measure the diffusivity of atomic hydrogen in an amorphous aIumina coating at room temperature using an electrochemical approach, to get a conservative estimate of the permeation. The effect of

hydrogen charging on the mechanical properties of the alumina coating–substrate system has not yet been studied. We analyzed the impact of hydrogen on the mechanical behavior and damage evolution in a Fe-8 wt% Cr alloy, hereafter referred to as Fe-8Cr, coated with alumina. To carry out this study, we used a combination of backside electrochemical hydrogen charging during in situ nanoindentation, scratch testing, atom probe tomography, and transmission electron microscopy. The backside charging approach is elucidated in the experimental section. This approach to charging is opposite to what is expected in service conditions, where gaseous hydrogen is in contact with the coating. We employed this reverse approach as an accelerated method to look at changes in the interface behavior/performance. It is possible that percolating paths to gaseous hydrogen can form in the coating through in-service wear and tear in practical situations. In this case, an accumulation of hydrogen may result in the interface. Our study aims to examine the mechanical behavior of coatings in such extreme situations.

Results and discussion

The as-deposited alumina coating shows a broad peak marked in the XRD data (Fig. 1a), indicative of the amorphous nature of the coating. Sharp reflections from the underlying BCC Fe-8Cr substrate are also observed. Additionally, in Fig. 1b, bright-field transmission electron microscopy (BF-TEM) suggests that the coatings are homogenous, and selected area diffraction (SAD) confirmed the amorphous structure of the alumina coatings.

Further investigation (supplementary S1) revealed that there exists a nearly 10-nm-thick crystalline structure of the coating at the steel substrate/coating interface. Regions that are farther away from the interface are clearly amorphous. It was also observed that long exposure to the electron beam at 200 kV led to crystallization of the amorphous oxide, which is consistent with the earlier observations [15]. Care was taken to avoid such imaging conditions to study the initial microstructure of the coatings without irradiation effects. Across the regions probed by TEM, there is no evidence of nanoscale defects such as pores or cracks which may be detrimental to the permeation and mechanical properties of the hydrogen barrier coating. The substrate has a large grain size of more than 100 µm. There is a surface region of 0.5–1 µm size formed by fine elongated grains (~ 200 nm) (Fig. 2b) as revealed by TEM. This zone is the result of mechanical polishing during sample preparation. STEM-EDS maps in Fig. 2 revealed that the coatings were exclusively composed of aluminum and

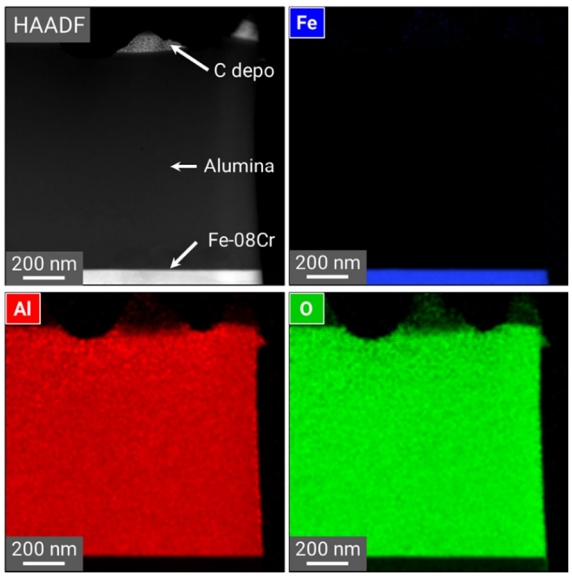

Figure 2: HAADF-STEM image and corresponding EDS maps show the elemental distribution in the as-deposited coating and substrate. A homogenous distribution of Al and O is present within the alumina.

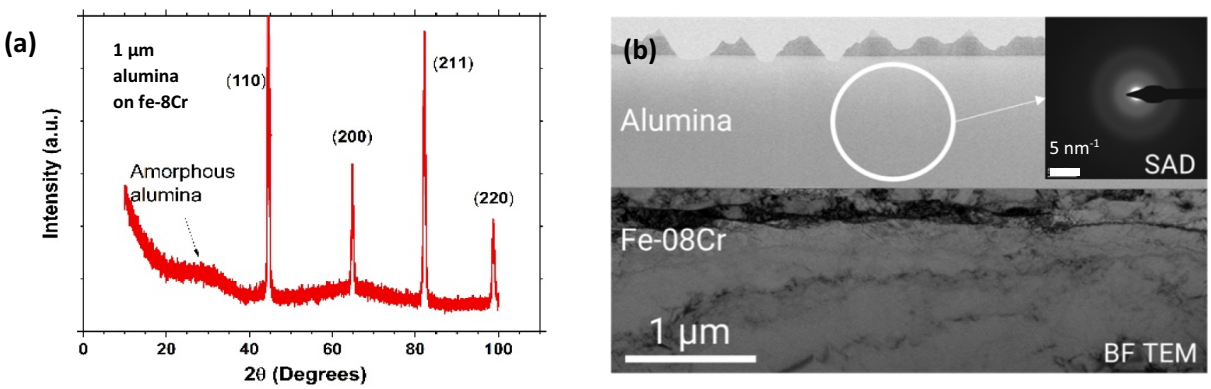

Figure 1: Microstructural characterization of the amorphous alumina coatings on Fe-8Cr. a) The X-ray diffractogram shows a broad amorphous peak corresponding to the alumina signal and sharp reflections from the Fe-8Cr substrate with a BCC structure. b) Bright-field TEM image of the coating and substrate, with an inset of selected area diffraction (SAD) from the coating, confirming its amorphous nature. The islands on top of the alumina coating are remains of the Pt/C protection layer used for milling.

oxygen, without any noticeable interdiffusion of iron or chromium atoms from the substrate.

The composition of the coating was further analyzed by APT in a region close to the substrate/coating interface, both prior and after hydrogen charging for 24 h. Figure 3a and b show 3D atom maps of H-charged and uncharged Al_2O_3, respectively. The APT reconstructions of both conditions did not show chemical partitioning, however, higher concentration of hydrogen species was measured in the H-charged specimen.

Table 1 shows the composition of H-charged and uncharged Al_2O_3 coatings. Each APT dataset contained > 27 million ions, as shown in the supplementary Figure S2. The Al-to-O ratios were 0.73 and 0.74 for the H-charged and uncharged specimens, respectively, which are slightly higher than the stoichiometric ratio of Al_2O_3 (0.6). The loss of oxygen detection has been commonly reported in oxide materials. This could be attributed to the recombination of oxygen ions on the tip surface, leading to the release of neutral molecular oxygen (O_2), which is not detectable in APT [16, 17]. The H-charged specimen contains two times higher hydrogen concentration than the uncharged specimen. It is important to focus only on the relative values of hydrogen in the H-charged sample compared to the uncharged one, rather than the absolute numbers. This has been widely discussed elsewhere [18–20]. In other words, the absolute numbers of hydrogen concentrations depicted in Table 1 are meaningless, and only the relative comparison is relevant. The elemental distribution in 5 samples (2 H-charged and 3 uncharged samples) is displayed in the supplementary figure S2, together with the mass spectra and charge-state ratios. The APT data confirm that hydrogen permeation through the Fe-8Cr substrate is successful

TABLE 1: Content of H detected by APT in H-charged and uncharged Al_2O_3.

Element	H-charged [at.%]	Uncharged [at.%]
Al	37.1 ± 0.1	39.8 ± 0.1
O	50.8 ± 0.1	53.7 ± 0.1
H	12.0 ± 0.2	6.4 ± 0.2

Note that hydrogen detected by APT may originate from sample preparation defects, pre-existing material content, or vacuum chamber measurements, with significant differences at similar electric fields (i.e., charge-state ratio) indicating intended hydrogen introduction for the H-charged sample.

and effectively reaches the alumina coating in the proximity of the interface. Hydrogen diffusivity in pure and undeformed α-Fe is reported to be 10^{-8} m^2s^{-1} [21, 22]. Grabke et al. [21] further report the diffusivity of Fe-10.4 Cr alloy as ~ 10^{-9} m^2s^{-1}. For a BCC Fe-20 wt% Cr alloy, with a higher Chromium content, we found the hydrogen diffusivity to be 10^{-10} m^2s^{-1} [13]. This relatively quick transport of hydrogen through the BCC lattice is expected for the Fe-8Cr alloy, leading to hydrogen reaching the coating from the backside in a short time. In addition, blisters were observed due to charging, suggesting localized interfacial hydrogen accumulation, as shown in supplementary figure S5.

Figure 4 displays the KP permeation curves for pure Fe-8Cr and the coated Fe-8Cr with a 78-nm-thick Al_2O_3 layer. The displayed hydrogen content in the additionally deposited Pd layer, $c(H_{Pd})$, was calculated from the measured potential values based on the Nernst equation [12]. The Kelvin probe technique is very sensitive to changes in the surface potential due to hydrogen permeation. Permeation caused by hydrogen evolution at the

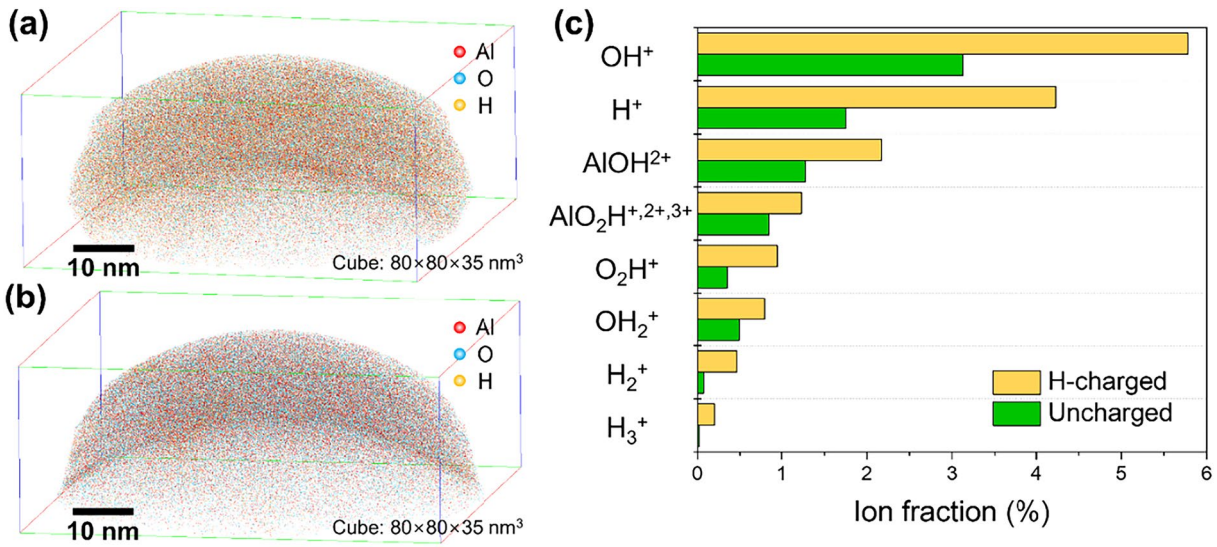

Figure 3: 3D atom maps of (a) H-charged and (b) uncharged Al2O3 specimens. (c) H and H-bonded polyatomic ion fractions of measured APT specimens.

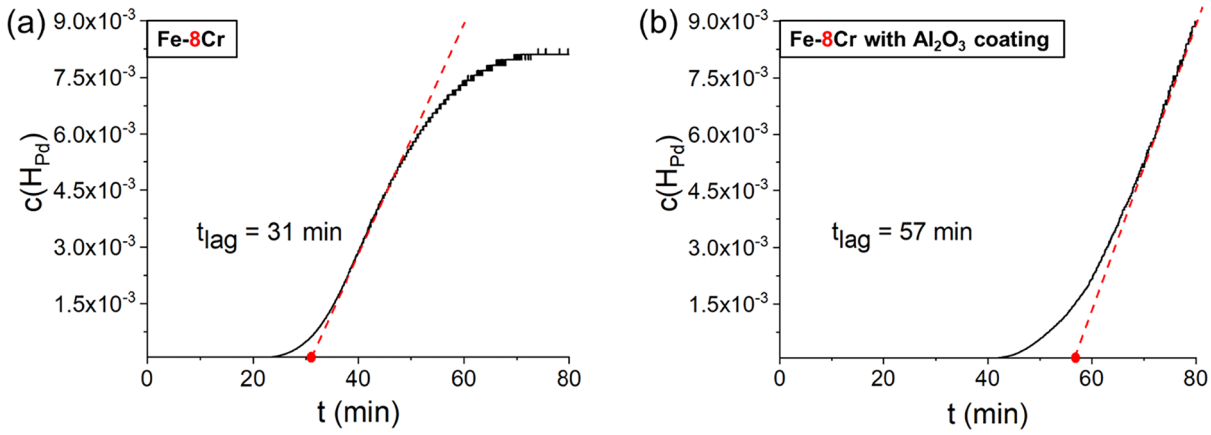

Figure 4: Hydrogen permeation curves obtained by KP-based hydrogen permeation tests at -1.52 VRef for (a) Fe-8Cr bare substrate and (b) Fe-8Cr coated with a 78 nm Al2O3 coating. The dotted red line represents the slope corresponding to the steady-state rate for hydrogen permeation, while its intersection with the x-axis indicates the lag time (tlag).

entry side of the sample can be easily detected at current densities well below 0.5 μA/cm^2 [23]. In addition, a low hydrogen release rate of up to 7 pA/cm^2 has also been evaluated within a small area of less than 0.1 mm^2 [24]. The lag time of 31 and 57 min, corresponding to the uncoated and Al_2O_3-coated (78 nm thickness) Fe-8Cr substrate, respectively, were used to calculate the apparent diffusion coefficients based on Eqs. 1–3 [1].

$$D_s = \frac{d_s^2}{t_{lag}} \tag{1}$$

$$D_{eff} = \frac{\left(d_s + d_f\right)^2}{t_{lag-eff}} \tag{2}$$

$$\frac{D_{eff}}{D_s} = \frac{\left(1 + \frac{d_s}{d_f}\right)^2}{\frac{D_s}{D_f} + 3\left(\frac{d_s}{d_f}\right)^2} \tag{3}$$

where D, t_{lag}, and d represent diffusivity, time(lag), and thickness, respectively, and the subscripts s, f, and eff stand for substrate, film, and effective (from the substrate and film together). The time-lag-based transient diffusivity measurement can be used to determine the diffusivity of the coating, with the assumption that the coating diffusivity is much smaller than substrate diffusivity [1]. Using the above expressions, the apparent diffusion coefficient of $4.40 \pm 0.11 \times 10^{-10}$ m^{2}s^{-1} for the substrate Fe-8Cr, and $2.39 \pm 0.06 \times 10^{-10}$ m^{2}s^{-1} for Fe-8Cr with 78-nm-thick Al_2O_3 coating were calculated. The hydrogen permeation time was 26 min delayed by the Al_2O_3 coating and the substrate/coating interface. By considering only the 78 nm Al_2O_3 coating thickness, the calculation of the apparent diffusivity of the Al_2O_3 coating yields 6.50×10^{-19} m^{2}s^{-1}. Based on these data, hydrogen permeation through 1-μm-thick alumina coating would require at least about 72 h to reach a steady state of the hydrogen flux, and therefore observe noticeable changes in the mechanical behavior of the coating. The primary interest in the current work is, however, to analyze the effect of hydrogen at the coating/substrate interface, which is the region most susceptible to failure in the studied system. The charging conditions for mechanical testing were therefore selected as 24 h, to introduce enough hydrogen at the interface without compromising the coating, and thus understand failure initiation.

Nanoindentation hardness and modulus data, shown in supplementary table S1, were virtually identical for the uncharged and the hydrogen-charged specimens with 1-μm-thick coating. Additional details are included in the supplementary section.

The examination of the scratch surface morphology and damage evolution through post-mortem SEM imaging reveal that hydrogen exposure leads to drastic changes in the scratch damage behavior, as shown in Fig. 5. The damage features were classified in three types according to their morphology: radial, lateral, or edge cracks. In the as-deposited coatings, the damage features start with *edge cracks*, which are parallel and close to the edge of the scratch track. The surface cracks within the scratch track are subdued. The *radial cracks*, which move away from the scratch track, occur at higher loads. Increasing the scratch peak load to 80 mN for the as-deposited conditions makes the damage features more prominent but does not alter the general behavior (supplementary figure S7). During hydrogen charging, edge cracks are suppressed, and *lateral surface cracks* perpendicular to the scratch direction become prominent within scratch track. Furthermore, the radial cracks are the first damage features that appear, occurring at reduced loads with respect to the as-deposited

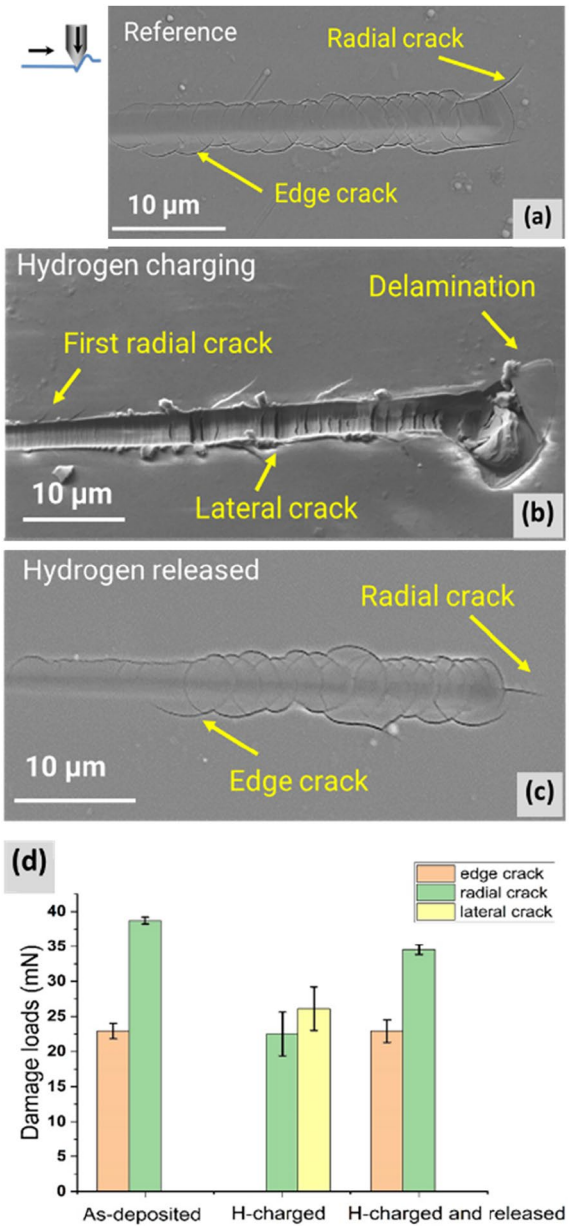

Figure 5: Representative SEM images of the scratch track a) in the as-deposited condition, b) during in situ hydrogen charging, and c) hydrogen charged and released. d) Damage loads for different crack patterns (edge, radial, and lateral) in the initial as-deposited coating state, during hydrogen exposure and after hydrogen release for two months in air at room temperature.

coatings. Interestingly, the different damage types occur at similar onset loads without and during hydrogen charging as shown in Fig. 5d. All scratch data, including damage onset loads, are summarized in supplementary table S1.

Post-mortem TEM examination of the scratch track also reveals different mechanisms of damage evolution in the as-deposited and hydrogen-charged coatings. In the as-deposited coatings (Fig. 6a), damage begins at the substrate–coating interface, and then grows upwards into the coating. It is also observed that damage initiates in sharp-ragged features that appear at the substrate, and most cracks do not extend to the surface. These sharp features did not exist prior to the scratching, and may be the result of plastic deformation localization during scratching. At higher loads (peak load of 80 mN), cracking becomes more evident, however, it follows the same pattern as previously observed.

During hydrogen charging (Fig. 6b), the damage features start from the coating and grow towards the substrate. However, most cracks stop before reaching the substrate and the cracks that reach the substrate are arrested at the interface without causing extensive delamination. This behavior is very promising for maintaining long-range structural integrity of the coatings over the substrate. Local delamination is also observed at the interface. Substrate plastic deformation occurs beneath the indenter and at the indenter front. The damage morphology and the mechanical behavior of the scratches in the specimens tested after 2 months of hydrogen release were similar to the as-deposited coatings, as shown in Fig. 5c. This indicates that hydrogen trapped at or near the interface is likely released, and the original mechanical behavior is recovered.

Hydrogen permeation data and the accompanying mechanisms are typically determined at high temperatures and pressures, where the diffusion-limited mechanism is thought to be dominant. However, it is recognized that at lower pressures and temperatures, the surface-limited mechanism may become the rate-controlling factor [1]. Experimental challenges associated with ascertaining this mechanism are daunting [1]. Therefore, as a conservative estimate, we measured diffusion-limited permeation, recognizing fully well that in reality for gaseous hydrogen through pipeline transport, the surface-limiting permeation can be slower and rate controlling. The diffusivity of the amorphous alumina coating at room temperature was calculated to be 6.5×10^{-19} m^2s^{-1}. To the best of the authors' knowledge, this is the first report of hydrogen diffusivity at room temperature in amorphous alumina or any other hydrogen barrier coating. The supplementary text contains a simple theoretical calculation of the hydrogen diffusivity at room temperature in native oxide film in aluminum. This estimate of 6.5×10^{-20} m^2s^{-1} for the native aluminum oxide is within one order of magnitude lower with respect to the measured diffusion coefficient in the deposited coating. Considering that the native oxide is adherent and strong, it is expected that its diffusivity is smaller compared to deposited amorphous alumina.

It is well recognized that the scratch behavior of coatings depends on the interfacial properties and on ratio of coating to substrate hardness [25]. Bull and Berasetegui [25] suggest that for a hard coating on a soft substrate, the coating's mechanical properties are primarily determined by the extensive plastic deformation of the substrate. Furthermore, interfacial hydrogen

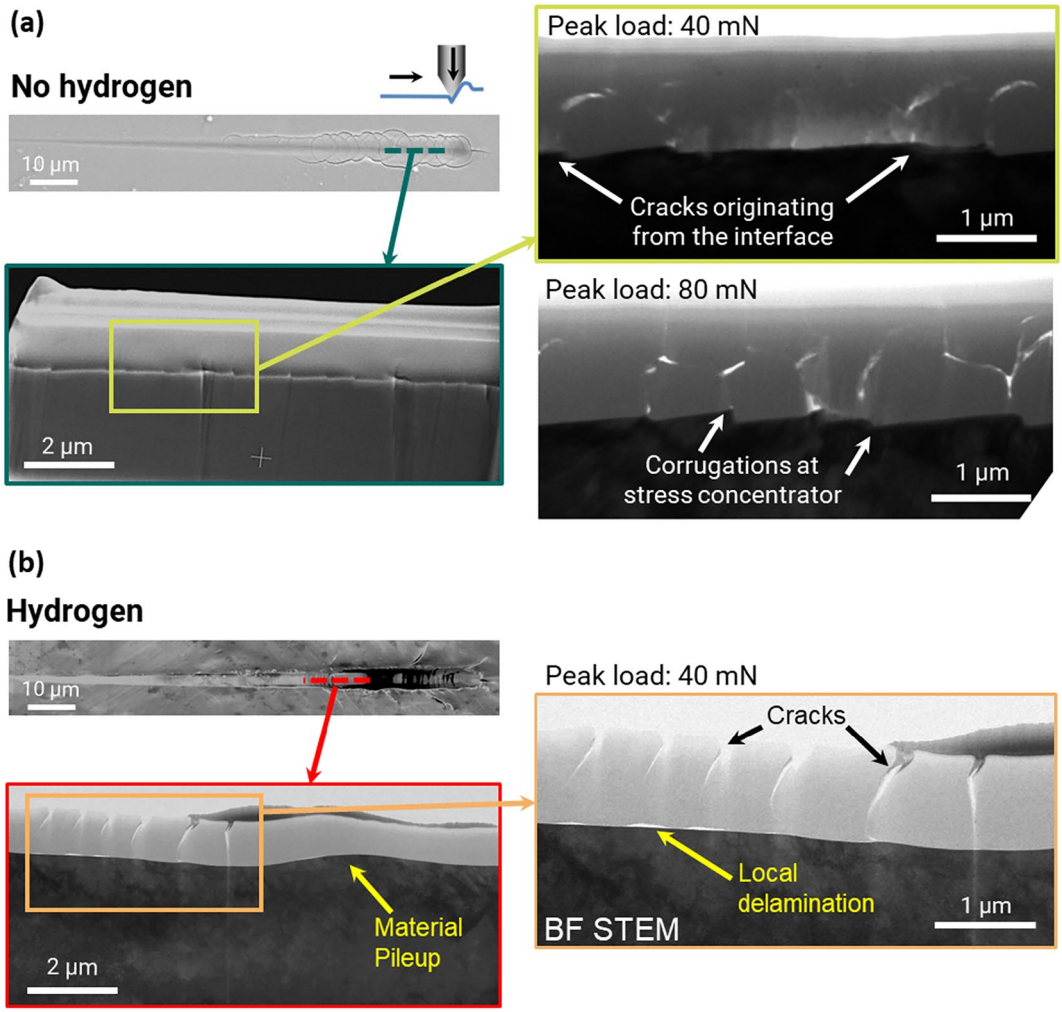

Figure 6: Damage evolution along the scratch track observed through top-view SEM and cross-sectional TEM. a) SEM image revealing the scratch morphology and overview SEM image of the coating/substrate region (left) with BF-TEM imaging of the scratch damage in the as-deposited coating for 40 and 80 mN peak loads, showing similar damage features in both cases (right). b) SEM and BF-STEM images of the coating scratch damage originated by scratching during in situ hydrogen charging. Note the local delamination at the coating/substrate interface in b) which is absent in a).

accumulation and resulting blister formation have been recognized in the literature [26, 27]. Hydrogen is known to segregate to interfaces and separate even metal from its native oxide [28]. We observed isolated blisters due to hydrogen charging, therefore the accumulation of hydrogen at the film-substrate interface can also lead to changes in load transfer to the substrate-coating system. Hydrogen gas pressure build-up at the interface due to continuous hydrogen supply in the in situ charged case can lead to damage features such as lateral cracks. Localized hydrogen enrichment in the coating, observed through APT experiments, confirms that the observed changes in the mechanical behavior could be related to hydrogen-induced changes to the substrate and interface. It is challenging to determine the influence of hydrogen on the intrinsic mechanical behavior of the amorphous alumina coating due to the lack of hydrogen diffusion to the top surface in the short time used for hydrogen charging in the current experiments. However, the scratch and hardness tests performed indicate that the coatings have good structural integrity under hydrogen charging conditions.

Conclusion

Hydrogen diffusivity and interface mechanical behavior were ascertained for an amorphous alumina coating deposited on a Fe-8 wt% Cr substrate. The samples were charged with hydrogen using an electrochemical backside charging setup, forcing the hydrogen to diffuse through the metal into the amorphous barrier coating. Based on Kelvin-Probe measurements, a hydrogen diffusivity of 6.50×10^{-19} m^2s^{-1} was obtained at room temperature for the amorphous alumina coating. The slow hydrogen diffusion in the alumina leads to accumulation of hydrogen at the coating/substrate interface in the studied approach. However,

even upon scratch testing the coating still adheres to the substrate. The scratch-induced cracks in the coating were different for the uncharged and hydrogen-charged specimens. The backside charging leads to debonded coating/substrate interface areas with lateral and radial cracks stopping within the coating. At very similar loads, edge and radial cracks evolve in the as-deposited coating. Interestingly, the scratch-induced cracking behavior completely recovered to the original behavior after hydrogen is released at ambient conditions. Nanoindentation did not pick-up any change in hardness and modulus for the hydrogen-exposed coating with respect to the as-deposited one. These aspects are promising to explore the amorphous alumina coating further for hydrogen barrier applications, while nanoindentation-based scratch tests can act as a quick sensor to resolve hydrogen-assisted degradation of the coating's mechanical performance.

Experimental details

Material synthesis

Plasma ion-assisted deposition (PIAD) [9] was employed to deposit amorphous alumina coatings on a 2-mm-thick Fe-8Cr substrate, which was polished up to 1 µm diamond suspension. The substrate was pre-heated to 170 °C and the depositing rate was 0.2 nm/s, while the sample rotated at 30 turns/min.

Microstructure characterization

Grazing incidence X-ray diffraction (XRD) was performed in a Rigaku SmartLab device with a CuK_{α} source to determine whether the deposited coatings were amorphous or crystalline. Microstructural changes and damage evolution due to hydrogen charging and mechanical testing were recorded by scanning electron microscopy (SEM) and transmission electron microscopy (TEM). SEM was performed in a Gemini 500 Zeiss microscope with an accelerating voltage of 5 kV using secondary electrons. Conventional TEM and scanning TEM (STEM) were carried out using a JEOL 2200 instrument operating at 200 kV accelerating voltage and a probe aberration-corrected Titan Themis (60-300kV) microscope from Thermo Fisher. Different detectors were employed for STEM imaging, specifically a bright-field (BF) detector and a high-angle annular dark-field (HAADF) detector covering angular regimes of < 7 mrad and 73-352 mrad, respectively. Energy-dispersive X-ray spectroscopy (EDS) analysis was conducted with a SuperX detector from Bruker attached to the Titan Themis. Site-specific TEM lamellae were prepared by Ga focused-ion beam (FIB) milling (ThermoFisher Scios) using a modified version of the procedure described in [10]. FIB milling was first performed at 30 kV acceleration voltage and 0.1 nA beam current, then the final polishing was conducted at 2 kV and 16 pA. A Pt/C protection layer was deposited on the alumina coating to prevent damage during FIB milling.

Atom probe tomography (APT) was performed on both uncharged and hydrogen-charged specimens to detect if any residual hydrogen remained bound to the alumina coating as a result from electrochemical charging. The samples were stored in a dry box at room temperature and the APT experiments were performed on the hydrogen-charged specimens a few weeks after hydrogen charging. While mobile hydrogen can escape, deeply trapped hydrogen will remain. The APT specimens were fabricated following the protocols described in [11]. APT analyses were performed using a local electrode atom probe (CAMECA LEAP 5000 XS) in a pulsed laser mode at a specimen base temperature of 60 K. The laser pulse energy, detection rate, and frequency were set to 30 pJ, 1%, and 125 kHz, respectively. Data reconstruction and analyses were done with the IVAS 3.8.8 software, provided by CAMECA Instruments. To avoid possible artifacts due to Ga implantation or surface contamination, the surface layer was excluded from the compositional analysis. For both, uncharged and hydrogen-charged specimens, APT tips were prepared from the coating layer near the substrate-coating interface. The cylindrical volume extracted from each atom map has a diameter of 30 nm and a length of 5 nm. Several specimens were investigated for each type of sample to ensure reliability.

Permeation tests

The Kelvin-probe (KP)-based in situ potentiometric hydrogen electrode method was used to quantify the hydrogen diffusion coefficient on the ferritic Fe-8Cr alloys with and without the Al_2O_3 coating at room temperature. The thickness of the Fe-8Cr specimen was ~ 2 mm, which is the same as the sample used for scratch and nanoindentation tests. The Al_2O_3 coating used to measure the diffusion coefficient had a thickness of 78 nm and was deposited on a ~ 2 mm Fe-8Cr substrate using the PIAD strategy described earlier. This thinner coating (78 nm thickness), compared to the ones used for mechanical testing (2 µm thickness), was employed to ensure a feasible experimental time during KP testing. To conduct a reliable permeation test, a 100 nm Pd layer was additionally deposited on top of the Al_2O_3 layer by physical vapor deposition (Leybold Univex 450). The changes in the surface potential related to hydrogen were then measured by KP over this Pd layer. Similar electrolyte and hydrogen charging conditions as the ones used for in situ mechanical testing were adopted for the permeation measurements. To promote the hydrogen evolution reaction, a potential of − 1.52 V_{Ref} was applied continuously on the bare Fe-8Cr substrate side, in contact with the electrolyte (Fig. 1) containing 0.1M NaOH and 20 mg/L As_2O_3. The hydrogen content in the Pd layer ($c(H_{Pd})$) was obtained by converting the measured KP potential (E) using the Nernst equation [12]:

$$E = E^{*\prime}_{SHE} + m \cdot \ln(c(H_{Pd})) \quad (4)$$

where $E^{*\prime}_{SHE}$ is the potential for standard hydrogen electrode, m is -130 mV/decade for this specific 100 nm Pd coating [12].

Scratch testing and nanoindentation

Mechanical properties were studied by nanoindentation with a diamond Berkovich tip without and during electrochemical hydrogen charging on an Agilent/KLA G200 nanoindenter. The continuous stiffness measurement (CSM) option was adopted to determine the hardness and modulus of the coatings. An oscillatory displacement signal of 2 nm with a frequency of 45 Hz was superimposed, with a total displacement of 200 nm into the coating. All indentation experiments were performed at an indentation strain rate ($\frac{h}{h}$.) of 0.05 s^{-1}. The average values were reported in the range of 50–100 nm to keep the overall displacement between 5 and 10% of the coatings. Additionally, one set of experiments was performed to a maximum displacement of 100 nm without the CSM option to cross check for the validity of the CSM measurement. At least 25 indentation measurements were performed for every condition.

Scratch tests were conducted to observe the effects of hydrogen exposure on the failure mechanisms of the coatings. Scratch tests using a 1 µm spherical diamond indenter tip were performed without and during hydrogen charging with a continuously increasing load ramp up to 40 mN, at a scan velocity of 1 µm s^{-1} and over a distance of 100 µm. Limited experiments on the uncharged specimen were additionally performed at 80 mN to observe the influence of peak load on the scratch behavior. All scratch tests were repeated at least 6 times to ensure reproducibility.

The hydrogen evolution reaction was promoted on the bare Fe-8Cr substrate side by adopting the novel electrochemical backside charging approach developed by Duarte et al. [13]. Figure 7 shows a schematic of the sample mounted on the backside hydrogen (H)-charging cell and how hydrogen diffuses from the bottom surface towards the coating. This ensures that the alumina coating would be exposed to hydrogen permeating through the alloy substrate. This prevents corrosion effects on the coating and provides insights into the interface stability between the Fe-8Cr substrate and alumina layer. Continuous hydrogen pre-charging was adopted for 24 h in the backside hydrogen cell. After this time, either nanoindentation or scratch tests were initiated, with the electrochemical hydrogen charging continuing to ensure constant hydrogen supply and prevent possible hydrogen loss. The electrolyte used is in hydrogel form, containing 0.1 M NaOH with an addition of 20 mg/L As_2O_3 to inhibit the hydrogen recombination reaction. After conducting cyclic sweep voltammetry tests, a constant voltage of – 1.44 V_{Ref}, corresponding to a measured current density of 1.5 mA/cm^2, was applied to promote the hydrogen evolution reaction, while inhibiting the excess formation of hydrogen bubbles. Additional details can be found here [14].

The scratch experiments were repeated on the same previously charged coated samples two months after the initial hydrogen charging and subsequent release at room temperature, to study if the observed effects were reversible. To verify that our in-house custom-built electrochemical hydrogen charging (backside) cell does not influence the hardness and modulus measurements, we performed nanoindentation tests on the mounted sample on the cell but with the electrochemical charging switched off and compared the results to the sample mounted on a standard stage.

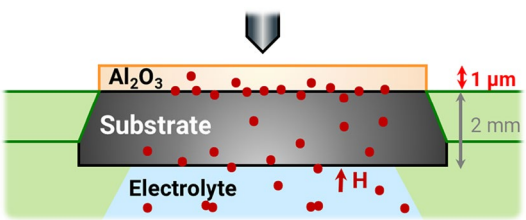

Figure 7: Schematic representation of the Al_2O_3-coated Fe-8Cr sample mounted on the backside charging electrochemical cell for in situ nanoindentation.

Acknowledgments

The authors would like to acknowledge Dr. Klaus Taube for feedback on the manuscript.

Author contributions

Hariprasad Gopalan: Investigation (nanoindentation, scratch testing, and SEM), data curation and analysis, writing original draft, and reviewing; Jing Rao: Investigation (Kelvin Probe and hydrogen charging) and analysis; Piyush Patil: Investigation (TEM); Chanwon Jung: Investigation, analysis, and writing (APT); Se-Ho Kim: Investigation and analysis (APT); Silas Goodrich: Investigation (TEM); Marcel Wetegrove: Thin film deposition and writing-related parts, reviewing; Angela Kruth: Conceptualization and project lead; Christina Scheu: Reviewing & editing manuscript, conceptualization, funding (PI), and project lead; Gerhard Dehm: Conceptualization, reviewing & editing manuscript, funding (PI) and project lead; Jazmin Maria Duarte: Conceptualization, data analysis and curation, reviewing & editing manuscript, and project lead.

Funding

Open Access funding enabled and organized by Projekt DEAL. The research project was carried out in the framework of the industrial collective research program (IGF no. 10859/18).

It was supported by the Federal Ministry for Economic Affairs and Climate Action (BMWK) through the AiF (German Federation of Industrial Research Associations eV) based on a decision taken by the German Bundestag.

Data availability

A reasonable request for raw data can be addressed to the corresponding authors.

Declarations

Conflict of interest On behalf of all authors, the corresponding authors state that there are no conflict of interest.

Supplementary Information

The online version contains supplementary material available at https://doi.org/10.1557/s43578-024-01348-y.

Open Access

References

1. V. Nemanič, Hydrogen permeation barriers: basic requirements, materials selection, deposition methods, and quality evaluation. Nucl. Mater. Energy **19**, 451–457 (2019)
2. E. Serra, A. Calza Bini, G. Cosoli, L. Pilloni, Hydrogen permeation measurements on alumina. J. Am. Ceram. Soc. **88**, 15–18 (2004)
3. D. Levchuk, F. Koch, H. Maier, H. Bolt, Deuterium permeation through Eurofer and α-alumina coated Eurofer. J. Nucl. Mater. **328**, 103–106 (2004)
4. M.A. Rosen, S. Koohi-Fayegh, The prospects for hydrogen as an energy carrier: an overview of hydrogen energy systems. Energy Ecol. Environ. **1**, 10–29 (2016)
5. S. Lynch, Hydrogen embrittlement phenomena and mechanisms. Corros. Rev. (2012). https://doi.org/10.1515/corrrev-2012-0502
6. E.J. Frankberg, J. Kalikka, F. Garcia, F. Joly-Pottuz, T. Salminen, H. Hokkasiddartha, K. Thierry, D. Berangere, L.S. Kreiml, M.J. Cordill, T. Epicier, D. Stauffer, M. Vanazzi, L. Roiban, J. Akola, F.D. Fonzo, E. Levanenand, K. Masenelli-Varlot, Highly ductile amorphous oxide at room temperature and high strain rate. Science **366**, 864–869 (2019)
7. Y. Yamada-Takamuraa, F. Koch, H. Maier, H. Bolt, Hydrogen permeation barrier performance characterization of vapor deposited amorphous aluminum oxide films using coloration of tungsten oxide. Surf. Coat. Technol. **153**, 114–118 (2002)
8. M. Wetegrove, M.-J. Duarte, K. Taube, M. Rohloff, H. Gopalan, C. Scheu, G. Dehm, A. Kruth, Preventing hydrogen embrittlement: the role of barrier coatings for hydrogen economy. Hydrogen **4**, 307–322 (2023)
9. O. Stenzel, J. Harhausen, D. Gäbler, S. Wilbrandt, C. Franke, R. Foest, N. Kaiser, Investigation on the reproducibility of optical constants of TiO2, SiO2, and Al2O3 films, prepared by plasma ion assisted deposition. Opt. Mater. Exp. **5**, 2006–2023 (2015)
10. M. Baram, W.D. Kaplan, Quantitative HRTEM analysis of FIB prepared specimens. J. Microsc. **232**, 395–405 (2008)
11. K. Thompson, D. Lawrence, D.J. Larson, J.D. Olson, T.F. Kelly, B. Gorman, In situ site specific specimen preparation for atom probe tomography. Ultramicroscopy **107**, 131–139 (2007)
12. C.-H. Wu, W. Krieger, M. Rohwerder, On the robustness of the Kelvin Probe based potentiometric hydrogen electrode method and its application in characterizing effective hydrogen activity in metal: 5 wt. % Ni cold-rolled ferritic steel as an example. Sci. Technol. Adv. Mater. **20**(1), 1073–1089 (2019)
13. M.J. Duarte, X. Fang, J. Rao, W. Krieger, S. Brinckmann, G. Dehm, In situ nanoindentation during electrochemical hydrogen charging: a comparison between front-side and a novel back-side charging approach. J. Mater. Sci. **56**, 8732–8744 (2021)
14. J. Rao, S. Lee, G. Dehm, M.J. Duarte, Hardening effect of diffusible hydrogen on BCC Fe-based model alloys by in situ backside hydrogen charging. Mater. Design **232**, 112143 (2023)
15. J. Murray, K. Song, W. Huebner, M. O'Keefe, Electron beam induced crystallization of sputter deposited amorphous alumina thin films. Mater. Lett. **74**, 12–15 (2012)
16. M. Karahka, Y. Xia, H.J. Kreuzer, The mystery of missing species in atom probe tomography of composite materials. Appl. Phys. Lett.. Lett. **107**, 062105 (2015)
17. B. Mazumder, X. Liu, R. Yeluri, F. Wu, U.K. Mishra, J.S. Speck, Atom probe tomography studies of Al2O3 gate dielectrics on GaN. J. Appl. Phys. **116**, 134101 (2014)
18. T.T. Tsong, T.J. Kinkus, C.F. Ai, Field induced and surface catalyzed formation of novel ions : a pulsed-laser time-of-flight atom-probe study. J. Chem. Phys. **78**, 4763 (1983)
19. C.-F. Ai, T.T. Tsong, Field promoted and surface catalyzed formation of H3 and NH3 on transition metal surfaces: a pulsed-laser imaging atom-probe study. Surf. Sci. **138**, 339–360 (1983)

20. B. Gault, D.W. Saxey, M.W. Ashton, S.B. Sinnott, A.N. Chiaramonti, M.P. Moody, D.K. Schreiber, Behavior of molecules and molecular ions near a field emitter. New J. Phys. Phys. **18**, 033031 (2016)
21. H.J. Grabke, E. Riecke, Absorption and diffusion of hydrogen in steels. Mater. Technol. **34**, 331 (2000)
22. K. Hirata, S. Iikubo, M. Koyama, K. Tsukazi, H. Ohtani, First-principles study on hydrogen diffusivity in BCC, FCC, and HCP iron. Metall. Mater. Trans. A **49A**, 5015–5022 (2018)
23. C. Senöz, S. Evers, M. Stratmann, M. Rohwerder, Scanning Kelvin Probe as a highly sensitive tool for detecting hydrogen permeation with high local resolution. Electrochem. Comm. **13**, 1542–1545 (2011)
24. S. Evers, C. Senöz, M. Rohwerder, Hydrogen detection in metals: a review and introduction of a Kelvin Probe approach. Sci. Tech. Adv. Mater. **14**, 014201 (2013)
25. S.J. Bull, E.G. Berasetegui, An overview of the potential of quantitative coating adhesion measurement by scratch testing. Tribol. Int. **39**, 99–114 (2006)
26. D.-G. Xie, Z.-J. Wang, J. Sun, J. Li, E. Ma, Z.-W. Shan, In situ study of the initiation of hydrogen bubbles at the aluminium metal/oxide interface. Nat. Mater. **14**, 899–903 (2015)
27. C.M. Lepienski, N.K. Kuromoto, J.F.P. Souza, C.E. Foerster, F.C. Serbena, S.L.R. Silva, Effect of hydrogen on mechanical properties of nitrided austenitic steels. Phil. Mag. **86**, 5407–5418 (2006)
28. M. Li, D.G. Xie, E. Ma, J. Li, X.-X. Zhang, Z.-W. Shan, Effect of hydrogen on the integrity of aluminium–oxide interface at elevated temperatures. Nat. Commun.Commun. **8**, 14564 (2017)